INTERNATIONAL JOURNAL FOR NUMERICAL METHODS IN ENGINEERING
Int. J. Numer. Meth. Engng 2009; **79**:667–695
Published online 25 February 2009 in Wiley InterScience (www.interscience.wiley.com). DOI: 10.1002/nme.2575

Optimization-based dynamic human walking prediction: One step formulation

Yujiang Xiang[‡], Jasbir S. Arora[*,†], Salam Rahmatalla and Karim Abdel-Malek

Virtual Soldier Research Program (*VSR*), *Center for Computer Aided Design* (*CCAD*), *College of Engineering*, *The University of Iowa*, *Iowa City*, *IA 52242*, *U.S.A.*

SUMMARY

A new methodology is introduced in this work to simulate normal walking using a spatial digital human model. The proposed methodology is based on an optimization formulation that minimizes the dynamic effort of people during walking while considering associated physical and kinematical constraints. Normal walking is formulated as a symmetric and cyclic motion. Recursive Lagrangian dynamics with analytical gradients for all the constraints and objective function are incorporated in the optimization process. Dynamic balance of the model is enforced by direct use of the equations of motion. In addition, the ground reaction forces are calculated using a new algorithm that enforces overall equilibrium of the human skeletal model. External loads on the human body, such as backpacks, are also included in the formulation. Simulation results with the present methodology show good correlation with the experimental data obtained from human subjects and the existing literature. Copyright © 2009 John Wiley & Sons, Ltd.

Received 9 May 2008; Revised 25 November 2008; Accepted 16 January 2009

KEY WORDS: gait analysis; ground reaction forces (GRF); recursive Lagrangian dynamics; zero moment point (ZMP); predictive dynamics

1. INTRODUCTION

Simulation of human walking is a challenging problem from analytical and computational points of view. Several attempts have been made in the past to develop realistic human walking using mechanical models. Many methods simulate human motion using databases generated from experiments on human subjects [1, 2]. Therefore, these approaches are limited by the accuracy and amount of available experimental data.

*Correspondence to: Jasbir S. Arora, Virtual Soldier Research Program (VSR), Center for Computer Aided Design (CCAD), College of Engineering, The University of Iowa, Iowa City, IA 52242, U.S.A.
†E-mail: jasbir-arora@uiowa.edu
‡E-mail: yujxiang@engineering.uiowa.edu

Contract/grant sponsor: TACOM
Contract/grant sponsor: Soldier Systems Center (Natick)

In addition to the database approach, some methods have attempted to model and simulate human walking. One well-known approach is the *zero moment point* (ZMP)-based trajectory generation method, which has received a great deal of attention. In this method, the walking motion can be generated in real time for smaller size models to follow the desired ZMP trajectory using an optimal control approach [3, 4]. The ZMP concept can also be incorporated in an optimization formulation to synthesize walking pattern by maximizing the stability, subject to physical constraints [5–7]. The key point of this approach is that the dynamics equations are used only to formulate the stability condition rather than generation of the entire motion trajectory directly, and so many dynamics details are not considered. Another approach is to solve the walking problem based on the idea that biped walking can be treated as an inverted pendulum. Advantages of this method are its simplicity and faster solvable dynamics equations [8]. However, the method also suffers from the inadequate dynamics model that cannot generate natural and realistic human motion.

Besides the foregoing approaches, optimization-based trajectory generation is another powerful simulation scheme. In this method, there is a better chance to achieve more realistic and natural human motion. In addition, the method can easily handle large degree of freedom (DOF) models, and can optimize many human-related performance measures simultaneously and satisfy all the constraints [9–14]. Chevallereau and Aoustin [9] planned robotic walking and running motions using optimization to determine the coefficients of a polynomial approximation for profiles of the pelvis translations and joint angle rotations. Saidouni and Bessonnet [10] used optimization to solve for cyclic, symmetric gait motion of a nine DOF model that moves in the sagittal plane; the control points for the B-spline curves along with the time durations for the gait stages were optimized to minimize the actuating torque energy. In another work, Anderson and Pandy [11] developed a musculoskeletal model with 23 DOFs and 54 muscles for normal symmetric walking on level ground. Muscle forces were treated as design variables and metabolic energy expenditure per unit distance was minimized. Lo *et al.* [12] determined human motion that minimized the summation of the squares of all actuating torques. The design variables were the control points for the cubic B-spline approximation of joint angle profiles. Sensitivity of joint torque with respect to control points were analytically obtained by using recursive Newton–Euler formulation.

In a previous approach, authors developed an optimization-based approach for predicting three dimensional human gait motions on level and inclined planes [15]. The joint motion histories were calculated by minimizing the deviation of the trunk from the upright posture, subjected to some physical constraints. Time durations for various gait phases were also optimized. The joint torques and ground reaction forces (GRF) were not calculated; therefore, constraints on the joint strength could not be imposed. The present work differs from the foregoing paper in the following aspects: recursive Lagrangian formulation is used for kinematics and dynamics, joint torques and GRF are calculated using equations of motion, a more realistic skeletal model is used, the optimization formulation is physics-based where an energy-related objective function is minimized, and constraints on the joint torques are imposed. As a result, a more realistic human walking motion is obtained.

The proposed approach, called predictive dynamics [16], uses a digital human model that has 55 DOFs, 6 DOFs for global translation and rotation, and 49 DOFs representing the kinematics of the body. Each DOF corresponds to relative rotation of two body segments connected by a revolute joint. The well-established robotic formulation of the Denavit–Hartenberg (DH) method is used for kinematics analysis of the open- and closed-loop branched mechanical system. The resultant action of all the muscles at a joint is lumped and represented by the torque at each DOF.

DOI: 10.1002/nme

The approach is called predictive dynamics since the joint torques and angles are both treated as unknowns in the optimization problem. In addition, the cubic B-spline interpolation is used to represent the time history of the joint angle profiles and parameterize the optimization problem. Furthermore, the recursive Lagrangian formulation which is known for its computational efficiency is used to develop the equations of motion. The approach is also suitable for evaluation of the gradients in closed form that are needed in the optimization process. A unique feature of the optimization formulation is that the equations of motion are not integrated explicitly, but evaluated by inverse dynamics. The dynamic effort (performance measure) that is represented as the integral of the squares of all the joint torques is minimized. The dynamic balance is achieved by satisfying the ZMP constraint throughout the walking motion. The sequential quadratic programming (SQP) algorithm is used to solve the non-linear optimization problem. Results of the optimization problem, torque and joint profiles, are shown to be realistic when compared with experimental data for normal walking. Besides normal walking, three other cases of walking with a shoulder backpack are simulated.

Major contributions of the paper compared with the gait literature [9–15] are:

(1) A large DOF spatial human skeleton model based on the DH method is used.
(2) Joint torques are calculated using the inverse recursive Lagrangian dynamics approach.
(3) ZMP is calculated using equations of motion; GRF are also calculated.
(4) Effect of external loads (shoulder backpack) on normal walking is studied.

2. SPATIAL HUMAN SKELETAL MODEL

The kinematics relation of a spatial human model is represented by DH method, in which, 4×4 homogeneous transformation matrices relate two adjacent coordinate systems [17]. The DH transformation matrix includes rotation and translation and is a function of four parameters: θ_i, d_i, α_i, and a_i which relate coordinate frames i and $i-1$, depicted in Figure 1.

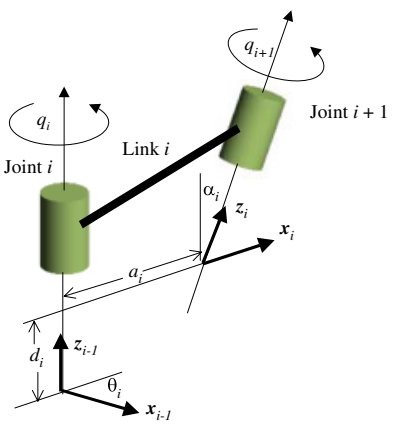

Figure 1. Joint coordinate systems.

DOI: 10.1002/nme

2.1. 55-DOF whole body model

A three-dimensional digital human skeletal model with 55 DOFs, shown in Figure 2 (the z's), has been developed by Virtual Soldier Research (VSR) program at the University of Iowa. The model consists of six physical branches and one virtual branch. The physical branches include the right leg, the left leg, the spine, the right arm, the left arm, and the head. In these branches, the right leg, the left leg, and the spine start from pelvis (z_4, z_5, z_6), while the right arm, left arm, and head start from the spine end joint (z_{30}, z_{31}, z_{32}).

The spine model includes four joints, each joint has three rotational DOFs ($[z_{21}, z_{22}, z_{23}]$, $[z_{24}, z_{25}, z_{26}]$, $[z_{27}, z_{28}, z_{29}]$, $[z_{30}, z_{31}, z_{32}]$). The legs and arms are assumed to be symmetric along

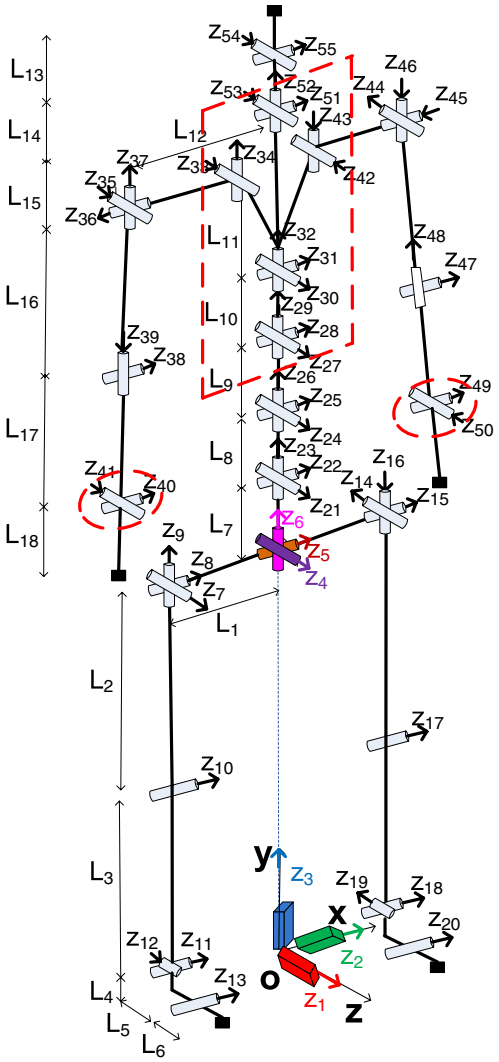

Figure 2. The 55-DOF digital human model (with global DOFs z_1, z_2, z_3, z_4, z_5, z_6).

DOI: 10.1002/nme

Table I. Link length and mass properties.

Link	Length (cm)	Mass (kg)
L_1	9.00	4.48
L_2	44.0	9.54
L_3	43.0	3.74
L_4	5.0	0.5
L_5	16.0	0.7
L_6	6.0	0.23
L_7	10.0	2.32
L_8	6.0	2.32
L_9	6.0	2.32
L_{10}	6.0	2.32
L_{11}	21.0	3.0
L_{12}	17.0	5.78
L_{13}	20.0	4.22
L_{14}	10.0	1.03
L_{15}	5.0	2.8
L_{16}	28.0	1.9
L_{17}	26.0	1.34
L_{18}	19.0	0.5

the sagittal plane. Each leg consists of a thigh, a shank, a rear foot, and a forefoot. There are seven DOFs for each leg: three at the hip joint (z_7, z_8, z_9), one at the knee joint (z_{10}), two at the ankle joint (z_{11}, z_{12}), and finally, one to characterize the forefoot (z_{13}). At the clavicle, there are two orthogonal revolute joints (z_{33}, z_{34}). Each arm consists of an upper arm, a lower arm, and a hand. There are seven DOFs for each arm: three at the shoulder, two at the elbow, and two at the wrist. In addition, there are five DOFs for the head branch: three at the lower neck, and two at the upper neck. The anthropometric data for the skeletal model representing a 50 percentile male, generated using GEBOD software [18], are shown in Table I.

It is noted here that the foregoing 55-DOF skeletal model has been developed to simulate many human activities, such as symmetric and asymmetric walking, running, stairs climbing, lifting objects, throwing, etc. For simulating each of these activities, some DOFs that do not participate in the activity in a significant manner are frozen to their neutral angles. The formulation presented here is quite flexible allowing any DOF to be frozen to a specified value. In addition, limits on the range of motion of any DOF can be imposed. A general purpose software is being developed that can be used to simulate these activities using the same skeletal model. For the symmetric gait simulation problem, the following DOFs are frozen: wrist joint, clavicle joint, neck joint, and two spine joints (shown as dashed enclosures in Figure 2). Therefore, the skeletal model used for gait simulation has 38 active DOFs. The other way accomplish this objective would be to redefine the skeletal model for each activity. However, this would require redefinition of the body segments and re-calculation of their mass and inertial properties which would be quite tedious.

2.2. Global DOFs and virtual joints

The six global DOFs generate rigid body motion for the entire spatial skeleton model. The three translations are represented by three prismatic joints and the three rotations by three revolution joints in the DH method. These joints are named as virtual joints to distinguish them from the

DOI: 10.1002/nme

physical human joints. The two adjacent virtual joints are connected by a virtual link which uses zero mass and zero inertia to define the link properties. Finally, the virtual joints and links constitute a virtual branch which contains six global DOFs $(z_1, z_2, z_3, z_4, z_5, z_6)$.

The virtual joints defined in the virtual branch not only generate global rigid body movements but also contain global generalized forces. These forces correspond to the six global DOFs: three forces (τ_1, τ_2, τ_3) and three moments (τ_4, τ_5, τ_6). For the system in equilibrium, these global generalized forces should be zero.

3. DYNAMICS MODEL

Recursive kinematics and Lagrangian approaches are adopted in this work to carry out the kinematics and dynamic analyses of the 3D human model instead of the regular Lagrangian formulation for the branched mechanical chains [19]. The reason for this adoption is the relative high computational cost associated with the regular Lagrangian formulation, of order $O(n^4)$ where n is the number of DOFs; in addition, the sensitivity cost is even larger. In contrast, computation cost of the recursive formulation is $O(n)$. In addition, it allows for setting up of the dynamic equations for the system in a recursive way [20, 21]. The sensitivity information about a joint involves only two adjacent joints; therefore, its computation cost is reduced to $O(n)$.

3.1. Forward recursive kinematics

In this process, 4×4 matrices $\mathbf{A}_j$, $\mathbf{B}_j$, $\mathbf{C}_j$ are defined to represent recursive position, velocity, and acceleration transformation matrices for the jth joint, respectively. Given the link transformation matrix $(\mathbf{T}_j)$ and the kinematics state variables for each joint, angular displacement, velocity, and acceleration ($q_j, \dot{q}_j$, and $\ddot{q}_j$), we have for $j=1$ to n:

$$\mathbf{A}_j = \mathbf{T}_1\mathbf{T}_2\mathbf{T}_3\ldots\mathbf{T}_j = \mathbf{A}_{j-1}\mathbf{T}_j \tag{1}$$

$$\mathbf{B}_j = \dot{\mathbf{A}}_j = \mathbf{B}_{j-1}\mathbf{T}_j + \mathbf{A}_{j-1}\frac{\partial \mathbf{T}_j}{\partial q_j}\dot{q}_j \tag{2}$$

$$\mathbf{C}_j = \dot{\mathbf{B}}_j = \ddot{\mathbf{A}}_j = \mathbf{C}_{j-1}\mathbf{T}_j + 2\mathbf{B}_{j-1}\frac{\partial \mathbf{T}_j}{\partial q_j}\dot{q}_j + \mathbf{A}_{j-1}\frac{\partial^2 \mathbf{T}_j}{\partial q_j^2}\dot{q}_j^2 + \mathbf{A}_{j-1}\frac{\partial \mathbf{T}_j}{\partial q_j}\ddot{q}_j \tag{3}$$

where $\mathbf{A}_0 = \mathbf{1}$ and $\mathbf{B}_0 = \mathbf{C}_0 = \mathbf{0}$. Then, the global position, velocity, and acceleration of a point in the Cartesian coordinate system can be calculated using the following formulas:

$$^0\mathbf{r}_j = \mathbf{A}_j\mathbf{r}_j, \quad ^0\dot{\mathbf{r}}_j = \mathbf{B}_j\mathbf{r}_j, \quad ^0\ddot{\mathbf{r}}_j = \mathbf{C}_j\mathbf{r}_j \tag{4}$$

where $^0\mathbf{r}_j$ and $\mathbf{r}_j$ are global and local augmented coordinates, respectively.

3.2. Backward recursive dynamics

Based on forward recursive kinematics, the backward recursion for the dynamic analysis is accomplished by defining a 4×4 transformation matrix $\mathbf{D}_i$ and 4×1 transformation vectors $\mathbf{E}_i$, $\mathbf{F}_i$, and $\mathbf{G}_i$ as follows: given the mass and inertia properties of each link, the external force

DOI: 10.1002/nme

$\mathbf{f}_k^{\mathrm{T}} = [{}^k f_x \ {}^k f_y \ {}^k f_z \ 0]$ and the moment $\mathbf{h}_k^{\mathrm{T}} = [{}^k h_x \ {}^k h_y \ {}^k h_z \ 0]$ for the link k, defined in the global coordinate system, the joint actuation torques τ_i for $i = n$ to 1 are computed as

$$\tau_i = \mathrm{tr}\left[\frac{\partial \mathbf{A}_i}{\partial q_i}\mathbf{D}_i\right] - \mathbf{g}^{\mathrm{T}}\frac{\partial \mathbf{A}_i}{\partial q_i}\mathbf{E}_i - \mathbf{f}_k^{\mathrm{T}}\frac{\partial \mathbf{A}_i}{\partial q_i}\mathbf{F}_i - \mathbf{G}_i^{\mathrm{T}}\mathbf{A}_{i-1}\mathbf{z}_0 \tag{5}$$

$$\mathbf{D}_i = \mathbf{I}_i\mathbf{C}_i^{\mathrm{T}} + \mathbf{T}_{i+1}\mathbf{D}_{i+1} \tag{6}$$

$$\mathbf{E}_i = m_i{}^i\mathbf{r}_i + \mathbf{T}_{i+1}\mathbf{E}_{i+1} \tag{7}$$

$$\mathbf{F}_i = {}^k\mathbf{r}_f\delta_{ik} + \mathbf{T}_{i+1}\mathbf{F}_{i+1} \tag{8}$$

$$\mathbf{G}_i = \mathbf{h}_k\delta_{ik} + \mathbf{G}_{i+1} \tag{9}$$

where $\mathbf{D}_{n+1} = \mathbf{0}$ and $\mathbf{E}_{n+1} = \mathbf{F}_{n+1} = \mathbf{G}_{n+1} = \mathbf{0}$; $\mathbf{I}_i$ is the inertia matrix for link i; m_i is the mass of link i; $\mathbf{g}$ is the gravity vector; ${}^i\mathbf{r}_i$ is the location of center of mass of link i in the local frame i; ${}^k\mathbf{r}_f$ is the position of the external force in the local frame k; $\mathbf{z}_0 = [0 \ 0 \ 1 \ 0]^{\mathrm{T}}$ for a revolute joint and $\mathbf{z}_0 = [0 \ 0 \ 0 \ 0]^{\mathrm{T}}$ for a prismatic joint; and finally, δ_{ik} is the Kronecker delta.

The first term in the torque expression (equation of motion) is the inertia and Coriolis torque, the second term is the torque due to gravity load, the third term is the torque due to external force, and the fourth term represents the torque due to the external moment.

3.3. Sensitivity analysis

The derivatives, $\partial\tau_i/\partial q_k$, $\partial\tau_i/\partial\dot{q}_k$, $\partial\tau_i/\partial\ddot{q}_k$ ($i = 1$ to n; $k = 1$ to n), can be evaluated for the articulated spatial human mechanical system in a recursive way using the foregoing recursive Lagrangian dynamics formulation as follows:

$$\frac{\partial\tau_i}{\partial q_k} = \begin{cases} \mathrm{tr}\left(\dfrac{\partial^2\mathbf{A}_i}{\partial q_i\partial q_k}\mathbf{D}_i + \dfrac{\partial\mathbf{A}_i}{\partial q_i}\dfrac{\partial\mathbf{D}_i}{\partial q_k}\right) - \mathbf{g}^{\mathrm{T}}\dfrac{\partial^2\mathbf{A}_i}{\partial q_i\partial q_k}\mathbf{E}_i - \mathbf{f}^{\mathrm{T}}\dfrac{\partial^2\mathbf{A}_i}{\partial q_i\partial q_k}\mathbf{F}_i - \mathbf{G}_i^{\mathrm{T}}\dfrac{\partial\mathbf{A}_{i-1}}{\partial q_k}\mathbf{z}_0 & (k \leqslant i) \\ \mathrm{tr}\left(\dfrac{\partial\mathbf{A}_i}{\partial q_i}\dfrac{\partial\mathbf{D}_i}{\partial q_k}\right) - \mathbf{g}^{\mathrm{T}}\dfrac{\partial\mathbf{A}_i}{\partial q_i}\dfrac{\partial\mathbf{E}_i}{\partial q_k} - \mathbf{f}^{\mathrm{T}}\dfrac{\partial\mathbf{A}_i}{\partial q_i}\dfrac{\partial\mathbf{F}_i}{\partial q_k} & (k > i) \end{cases} \tag{10}$$

$$\frac{\partial\tau_i}{\partial\dot{q}_k} = \mathrm{tr}\left(\frac{\partial\mathbf{A}_i}{\partial q_i}\frac{\partial\mathbf{D}_i}{\partial\dot{q}_k}\right) \tag{11}$$

$$\frac{\partial\tau_i}{\partial\ddot{q}_k} = \mathrm{tr}\left(\frac{\partial\mathbf{A}_i}{\partial q_i}\frac{\partial\mathbf{D}_i}{\partial\ddot{q}_k}\right) \tag{12}$$

More details about the derivation of sensitivity equations can be found in Xiang *et al.* [22].

3.4. Mass and inertia property

The forward kinematics transfers the motion from the origin toward the end effector along the branch as shown in Figure 3. This process only involves state variables and geometrical parameters. However, backward dynamics propagates forces from end effector to the origin, and the mass and inertia property of the links need to be considered for dynamic analysis.

DOI: 10.1002/nme

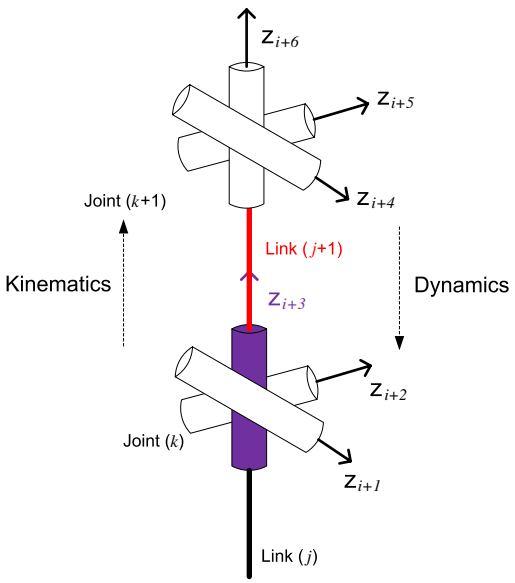

Figure 3. Mass and inertia allocation for joint pairs.

In Figure 3, joint (k) and joint $(k+1)$ are connected by link $(j+1)$ for which mass and inertia properties are defined in the local coordinate z_{i+3}. The links between coordinates z_{i+3} and z_{i+2}, and z_{i+2} and z_{i+1} have zero link length, and zero mass and inertia, so that the force is correctly transferred back through z_{i+3}, z_{i+2}, and z_{i+1} for the joint (k).

4. GAIT MODEL

4.1. One-step gait model

A complete gait cycle includes two continuous steps (one stride). In the current work, normal walking is assumed to be symmetric and cyclic; therefore, only one step of the gait cycle needs to be modeled and simulated. Each step is divided into two phases, single support phase and double support phase. Single support phase occurs when one foot contacts the ground while the other leg is swinging; it starts from the rear foot toe-off and ends when the swinging foot lands on the ground with a heel strike; the time duration for this phase is denoted as T_{SS}. Considering the ball joint of foot, the single support phase can be detailed into two basic supporting modes: rear foot single support and forefoot single support. The double support phase is characterized by both feet contacting the ground. This phase starts from the front foot heel strike and ends with the contra-lateral foot toe-off. The time duration of double support is denoted as T_{DS}. In this work, a walking step starts from left heel strike, then goes through left foot flat, right toe-off, right leg swing, left heel off, and finally comes back to right heel strike as shown in Figure 4. The foot support polygon is plotted in Figure 5. The foot contacting conditions are summarized in Table II.

DOI: 10.1002/nme

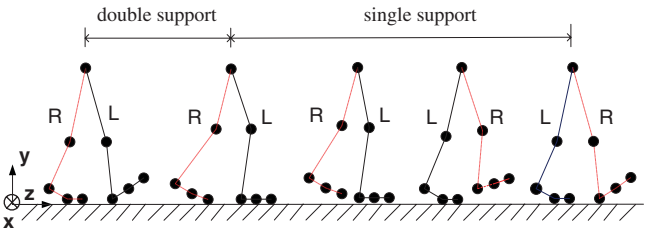

Figure 4. Basic feet supporting modes in a step (side view: *R* denotes right leg; *L* denotes left leg).

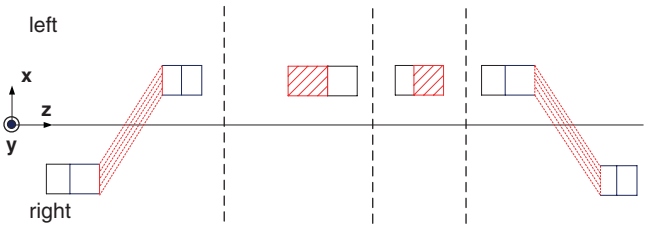

Figure 5. Foot support polygon (dash area) in a step.

Table II. Foot contacting conditions: four modes in a step.

	Single support		
Double support	Rear foot	Forefoot	Double support
Right toe Left heel	Left heel Left ball	Left ball Left toe	Left toe Right heel

Symmetry conditions for the gait cycle are needed so that only one step can be modeled to simulate gait. In the proposed approach, the successive step repeats the motion of previous step by swapping the roles of legs and arms. The initial and final joint angles and velocities (at left heel strike and subsequent right heel strike) should satisfy symmetry conditions so as to generate continuous and cyclic gait motion.

4.2. Two-step algorithm to calculate GRF

Inclusion of GRF in the gait formulation has two challenges: not only is the GRF value transient, but also the GRF position is variable. To solve these forces, a two-step algorithm is developed. First, we distinguish forces into two categories: active forces and GRF. Active forces include inertia, Coriolis, gravity, and external forces and moments. The main idea of the algorithm is to first calculate resultant of the active forces and ZMP location from the equations of motion and then calculate GRF using the global equilibrium conditions between the active forces and GRF. After that, the obtained GRF are applied as external loads at the ZMP, together with the active forces, to recover the real joint torques. This two-step algorithm is depicted in Figure 6 and explained as

DOI: 10.1002/nme

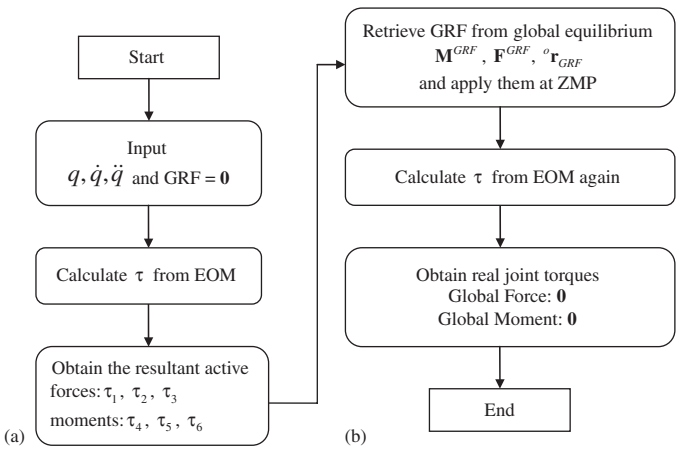

Figure 6. Flowchart of the two-step algorithm to obtain GRF and real joint torques.

follows:

Step 1: Given current state variables q, $\dot{q}$, and $\ddot{q}$, external loads and gravity, the joint torques are calculated using the inverse recursive Lagrangian dynamics without the GRF. This is illustrated in Figure 6(a). The global forces τ_1, τ_2, τ_3 and moments τ_4, τ_5, τ_6 in the virtual branch are not zero at this stage due to exclusion of GRF. These forces are in fact the resultants of the active forces at the end of the virtual branch, i.e. the pelvis. After that, the ZMP is calculated using these forces, as explained in the following subsection.

Step 2: This step is illustrated in Figure 6(b). Considering the global equilibrium between the resultant active forces and the GRF at ZMP, the resultant GRF are obtained and then treated as external forces applied at ZMP for the human model, such as the forces **f** and **h** in Equations (5)–(9). Given the state variables, external loads, gravity loads as well as the GRF, the real joint torques are recovered from the equations of motion using Equation (5).

4.2.1. Zero moment point (*ZMP*). ZMP is a well-known bipedal dynamic balance criterion that has been used quite widely in the area of robotics and biomechanics [23]. ZMP is the point on the ground where the resultant tangential moments of the active forces are zero. The position of ZMP can be calculated using the conditions: $M_z = 0$ and $M_x = 0$ (z is the walking direction, x is the lateral direction, and y is the vertical direction; refer to Figure 4).

$$x_{\text{zmp}} = \frac{\sum_{i=1}^{\text{nlink}} (m_i(-\ddot{y}_i + g)x_i + m_i \ddot{x}_i y_i - J_i \ddot{\theta}_{iz} + f_{iy}x_i - f_{ix}y_i + h_{iz})}{\sum_{i=1}^{\text{nlink}} m_i(-\ddot{y}_i + g)} \tag{13a}$$

$$z_{\text{zmp}} = \frac{\sum_{i=1}^{\text{nlink}} (m_i(-\ddot{y}_i + g)z_i + m_i \ddot{z}_i y_i + J_i \ddot{\theta}_{ix} + f_{iy}z_i - f_{iz}y_i - h_{ix})}{\sum_{i=1}^{\text{nlink}} m_i(-\ddot{y}_i + g)} \tag{13b}$$

where x_i, y_i, z_i are the global coordinates of the center of mass for the link i, m_i is the mass, J_i is the global inertia, $\ddot{\theta}_i$ is the global angular acceleration of link i, f_i and h_i are the external force and moment applied on link i, $g = -9.8062\,\text{m/s}^2$.

DOI: 10.1002/nme

To calculate ZMP, the inertia J_i and angular acceleration $\ddot{\theta}_i$ need to be evaluated in the global coordinates; however, they have been defined in the local coordinates associated with link i in the DH method. The transformation to the global coordinates is tedious and time consuming. Therefore, some researchers simply ignore these terms in ZMP calculation. Instead, in this work we develop an alternative method to calculate ZMP based on global equilibrium condition, or equivalently, the forces and moments in the virtual branch obtained from equations of motion. The basic idea is to use resultant of the active forces and moments to calculate ZMP directly instead of evaluating them link by link as in Equations (13).

Given state variables ($q_j, \dot{q}_j$, and $\ddot{q}_j$) for each joint, apply active forces to the mechanical system, excluding GRF. The calculated generalized forces (τ_1, τ_2, τ_3, τ_4, τ_5, τ_6) in the virtual branch from equations of motion are in fact the resultant active forces and moments. After obtaining resultant of the active forces, we can use them to calculate ZMP using the following three steps: (1) calculate resultant of the active forces and moments at the pelvis in the inertial reference frame; (2) transfer these forces and moments to the origin of the inertial reference frame (o-*xyz*); (3) calculate the ZMP from its definition.

(1) *Global forces at pelvis*: It should be noted that the direction of the resultant active moments (τ_5, τ_6) at the pelvis is defined in the local coordinates (z_5, z_6). They no longer align with the global Cartesian coordinates (o-*xyz*) because of the global rotational movements (q_4, q_5), as shown in Figure 7. As ZMP is defined in the global Cartesian coordinates, we need to recover the resultant active moments $\mathbf{M}^p = [M_x^p \quad M_y^p \quad M_z^p]^{\mathrm{T}}$ at pelvis in the global Cartesian coordinates which is done using the following equilibrium equation:

$$\begin{bmatrix} \cos(z_4, x) & \cos(z_4, y) & \cos(z_4, z) \\ \cos(z_5, x) & \cos(z_5, y) & \cos(z_5, z) \\ \cos(z_6, x) & \cos(z_6, y) & \cos(z_6, z) \end{bmatrix} \begin{bmatrix} M_z^p \\ M_x^p \\ M_y^p \end{bmatrix} + \begin{bmatrix} \tau_4 \\ \tau_5 \\ \tau_6 \end{bmatrix} = \mathbf{0} \tag{14}$$

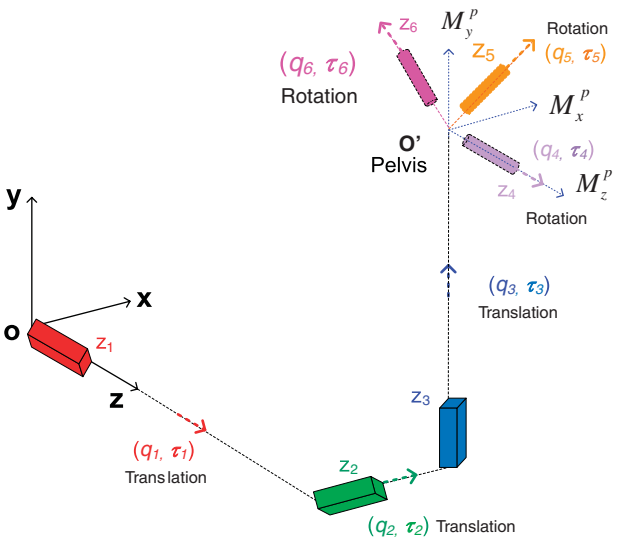

Figure 7. Global DOFs in virtual branch.

DOI: 10.1002/nme

where τ_4, τ_5, τ_6 are resultant moments along the DH local axes associated with their DOFs; $\cos(z_4, x)=0$, $\cos(z_4, y)=0$, and $\cos(z_4, z)=1$ because the first rotational joint is align with global z axis.

The resultant active forces $\mathbf{F}^p=[F_x^p \quad F_y^p \quad F_z^p]^{\mathrm{T}}$ at the pelvis are obtained by considering equilibrium between two sets of forces, as:

$$F_x^p+\tau_2=0; \quad F_y^p+\tau_3=0; \quad F_z^p+\tau_1=0 \tag{15}$$

(2) *Global forces at origin*: After obtaining the global forces at the pelvis in the global Cartesian coordinates we can transfer the resultant active force from pelvis to the origin using the equilibrium conditions. Thus, the resultant active forces $(\mathbf{M}^{\mathrm{o}}, \mathbf{F}^{\mathrm{o}})$ at origin are obtained as follows:

$$\begin{aligned} \mathbf{M}^{\mathrm{o}} &= \mathbf{M}^p + {}^{\mathrm{o}}\mathbf{r}_p \times \mathbf{F}^p \\ \mathbf{F}^{\mathrm{o}} &= \mathbf{F}^p \end{aligned} \tag{16}$$

where $\mathbf{M}^{\mathrm{o}}=[M_x^{\mathrm{o}} \quad M_y^{\mathrm{o}} \quad M_z^{\mathrm{o}}]^{\mathrm{T}}$ and $\mathbf{F}^{\mathrm{o}}=[F_x^{\mathrm{o}} \quad F_y^{\mathrm{o}} \quad F_z^{\mathrm{o}}]^{\mathrm{T}}$. ${}^{\mathrm{o}}\mathbf{r}_p$ is the pelvis position vector in the global coordinate system, as depicted in Figure 8.

(3) *ZMP calculation*: Next, the resultant active forces are further transferred from the origin to the ZMP by using the equilibrium conditions; i.e. $(\mathbf{M}^{\mathrm{zmp}}, \mathbf{F}^{\mathrm{zmp}})$ are obtained using the equation:

$$\begin{aligned} \begin{pmatrix} M_x^{\mathrm{zmp}} \\ M_y^{\mathrm{zmp}} \\ M_z^{\mathrm{zmp}} \end{pmatrix} &= \begin{pmatrix} M_x^{\mathrm{o}} \\ M_y^{\mathrm{o}} \\ M_z^{\mathrm{o}} \end{pmatrix} + \begin{pmatrix} x_{\mathrm{zmp}} \\ y_{\mathrm{zmp}} \\ z_{\mathrm{zmp}} \end{pmatrix} \times \begin{pmatrix} F_x^{\mathrm{o}} \\ F_y^{\mathrm{o}} \\ F_z^{\mathrm{o}} \end{pmatrix} \\ \mathbf{F}^{\mathrm{zmp}} &= \mathbf{F}^{\mathrm{o}} \end{aligned} \tag{17}$$

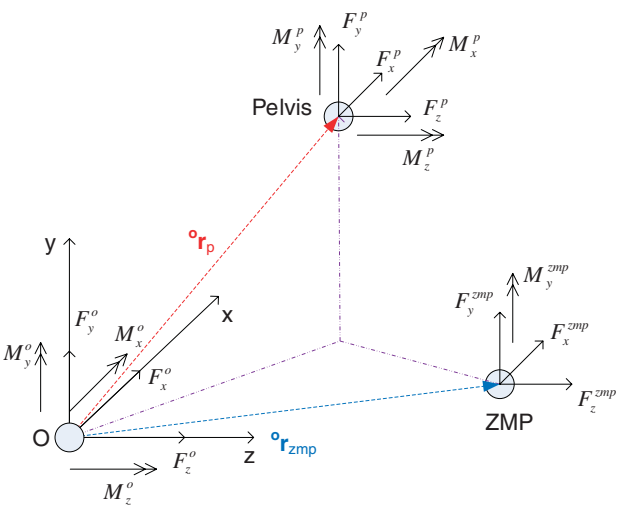

Figure 8. Resultant active forces at pelvis, origin and ZMP.

DOI: 10.1002/nme

where ${}^{\mathrm{o}}\mathbf{r}_{\mathrm{zmp}} = [x_{\mathrm{zmp}} \;\; y_{\mathrm{zmp}} \;\; z_{\mathrm{zmp}}]^{\mathrm{T}}$ is the ZMP position vector in the global coordinates. As ZMP is set on the level ground and tangential moments are zero due to its definition, we have:

$$y_{\mathrm{zmp}} = 0, \quad M_x^{\mathrm{zmp}} = 0, \quad M_z^{\mathrm{zmp}} = 0 \tag{18}$$

Using Equations (17) and (18), the ZMP position is uniquely obtained as follows:

$$x_{\mathrm{zmp}} = \frac{M_z^{\mathrm{o}}}{F_y^{\mathrm{o}}}, \quad z_{\mathrm{zmp}} = \frac{-M_x^{\mathrm{o}}}{F_y^{\mathrm{o}}} \tag{19}$$

In addition, the resultant active moment at ZMP along y axis is also obtained from Equation (17):

$$M_y^{\mathrm{zmp}} = M_y^{\mathrm{o}} + F_x^{\mathrm{o}} z_{\mathrm{zmp}} - F_z^{\mathrm{o}} x_{\mathrm{zmp}} \tag{20}$$

There are two major advantages of using the foregoing ZMP formulation: one is that calculation of resultant active forces from equations of motion is very convenient and straightforward; and the other is that the resultant active forces ($\mathbf{M}^{\mathrm{zmp}}, \mathbf{F}^{\mathrm{zmp}}$) and position ${}^{\mathrm{o}}\mathbf{r}_{\mathrm{zmp}}$ of the ZMP are obtained simultaneously. The resultant active forces at ZMP are used to calculate the GRF.

4.2.2. Ground reaction forces (*GRF*). The resultant GRF are located at the center of pressure which coincides with the ZMP as long as the dynamic system is in balance [24, 25]. Thus, the transient position of the resultant GRF can be obtained by tracing the ZMP position ${}^{\mathrm{o}}\mathbf{r}_{\mathrm{zmp}}$ using Equation (19). Moreover, the transient value of resultant GRF is also obtained from global equilibrium conditions as:

$$\begin{aligned} \mathbf{M}^{\mathrm{GRF}} + \mathbf{M}^{\mathrm{zmp}} &= \mathbf{0} \\ \mathbf{F}^{\mathrm{GRF}} + \mathbf{F}^{\mathrm{zmp}} &= \mathbf{0} \\ {}^{\mathrm{o}}\mathbf{r}_{\mathrm{GRF}} - {}^{\mathrm{o}}\mathbf{r}_{\mathrm{zmp}} &= \mathbf{0} \end{aligned} \tag{21}$$

In the single support phase, one foot supports the whole body and ZMP stays in the foot area so that GRF can be applied at the ZMP directly. However, in the double support phase, ZMP is located between the two supporting feet, and the resultant GRF needs to be distributed to the two feet appropriately. This partitioning process can be treated as a sub-optimization problem [26]. In order to simplify this process, the GRF is distributed to the points (A, B) of the supporting parts on each foot as shown in Figure 9, where point A (triangle) is the left toe center and point B (triangle) is the right heel center. d_1 and d_2 are the distances from ZMP (circle) to points A

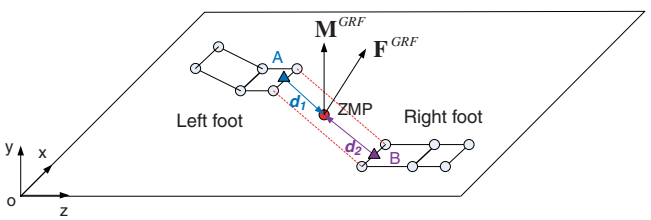

Figure 9. Partition of ground reaction forces.

DOI: 10.1002/nme

and B, respectively. A linear relationship is used to partition GRF. The GRF value is first linearly decomposed at ZMP as follows:

$$\begin{aligned} \mathbf{M}_1^{\mathrm{GRF}} &= \frac{d_2}{d_1+d_2}\mathbf{M}^{\mathrm{GRF}}, \quad \mathbf{F}_1^{\mathrm{GRF}} = \frac{d_2}{d_1+d_2}\mathbf{F}^{\mathrm{GRF}} \\ \mathbf{M}_2^{\mathrm{GRF}} &= \frac{d_1}{d_1+d_2}\mathbf{M}^{\mathrm{GRF}}, \quad \mathbf{F}_2^{\mathrm{GRF}} = \frac{d_1}{d_1+d_2}\mathbf{F}^{\mathrm{GRF}} \end{aligned} \tag{22}$$

Then, $(\mathbf{M}_1^{\mathrm{GRF}}, \mathbf{F}_1^{\mathrm{GRF}})$ are transferred to point A and $(\mathbf{M}_2^{\mathrm{GRF}}, \mathbf{F}_2^{\mathrm{GRF}})$ to point B as follows:

$$\begin{aligned} \mathbf{M}^A &= \mathbf{M}_1^{\mathrm{GRF}} + {}^A\mathbf{d}_{\mathrm{zmp}} \times \mathbf{F}_1^{\mathrm{GRF}} \\ \mathbf{F}^A &= \mathbf{F}_1^{\mathrm{GRF}} \end{aligned} \tag{23}$$

$$\begin{aligned} \mathbf{M}^B &= \mathbf{M}_2^{\mathrm{GRF}} + {}^B\mathbf{d}_{\mathrm{zmp}} \times \mathbf{F}_2^{\mathrm{GRF}} \\ \mathbf{F}^B &= \mathbf{F}_2^{\mathrm{GRF}} \end{aligned} \tag{24}$$

where ${}^A\mathbf{d}_{\mathrm{zmp}}$ is the position vector from point A to ZMP, and ${}^B\mathbf{d}_{\mathrm{zmp}}$ is the position vector from point B to ZMP.

5. OPTIMIZATION FORMULATION

For a given walking velocity (V) and a step length (L), the time duration for the step is calculated as $T = L/V$. The double support time duration is taken as $T_{\mathrm{DS}} = \alpha T$; as a result, the single support time duration is given as $T_{\mathrm{SS}} = (1-\alpha)T$. Single support is detailed into rear foot support (mid-stance) and forefoot support (terminal stance). Their time durations are set to βT_{SS} and $(1-\beta)T_{\mathrm{SS}}$, respectively. The parameters α and β are obtained from the literature [27].

The walking task is formulated as a non-linear programming optimization problem. A general mathematical form is defined as: find the optimal joint trajectories $\mathbf{q}(t)$ and joint torques $\boldsymbol{\tau}(t)$ to minimize a human performance measure subject to physical constraints:

$$\begin{aligned} \text{Find:}\ & \mathbf{q}, \boldsymbol{\tau} \\ \text{To:}\ & \min F(\mathbf{q}, \boldsymbol{\tau}) \\ \text{Sub.}\ & h_i = 0, \quad i = 1, \ldots, m \\ & g_j \leqslant 0, \quad j = 1, \ldots, k \end{aligned} \tag{25}$$

where h_i are the equality constraints and g_j are the inequality constraints.

5.1. Design variables

In the current formulation,the design variables are the joint angle profiles $\mathbf{q}(t)$. The joint torques $\boldsymbol{\tau}(\mathbf{q}, \mathbf{t})$ are calculated using the governing differential equations. This is called the inverse dynamics procedure where the differential equations are not integrated. This has also been called the differential inclusion formulation.

DOI: 10.1002/nme

5.2. Objective function

The predicted motion depends strongly on the adopted objective function F. In this work, the dynamic effort, the time integral of squares of all the joint torques, is used as the performance criterion for the walking problem:

$$F(\mathbf{q}) = \int_{t=0}^{T} \left(\frac{\boldsymbol{\tau}(\mathbf{q}, t)}{|\tau|_{\max}} \right)^{\mathrm{T}} \cdot \left(\frac{\boldsymbol{\tau}(\mathbf{q}, t)}{|\tau|_{\max}} \right) \mathrm{d}t \tag{26}$$

where $|\tau|_{\max}$ is the maximum absolute value of joint torque limit.

5.3. Constraints

Two types of constraints are considered for the walking optimization problem: one is the time-dependent constraints which include joint limits, torque limits, ground penetration, dynamic balance, arm–leg coupling, and self avoidance. These constraints are imposed throughout the time interval. The second type is time-independent constraints which comprise the symmetry conditions, ground clearance and initial and final foot positions; these constraints are considered only at a specific time point during the step.

5.3.1. Time-dependent constraints. (1) *Joint limits*: To avoid hyperextension, the joint limits are taken into account in the formulation. The joint limits representing the physical range of motion:

$$\mathbf{q}^{\mathrm{L}} \leqslant \mathbf{q}(t) \leqslant \mathbf{q}^{\mathrm{U}}, \quad 0 \leqslant t \leqslant T \tag{27}$$

where $\mathbf{q}^{\mathrm{L}}$ are the lower joint limits and $\mathbf{q}^{\mathrm{U}}$ the upper limits as given in Table AI.

Joint limit constraint is also used to 'freeze' a DOF by setting its lower bound and upper bound to the neutral angle (the natural angle at rest) instead of eliminating this DOF from the skeleton model.

(2) *Torque limits*: Each joint torque is also bounded by its physical limits which are obtained from the literatures [28–30]:

$$\boldsymbol{\tau}^{\mathrm{L}} \leqslant \boldsymbol{\tau}(t) \leqslant \boldsymbol{\tau}^{\mathrm{U}}, \quad 0 \leqslant t \leqslant T \tag{28}$$

where $\boldsymbol{\tau}^{\mathrm{L}}$ are the lower torque limits and $\boldsymbol{\tau}^{\mathrm{U}}$ the upper limits.

(3) *Ground penetration*: Walking is characterized with unilateral contact between the foot and ground as shown in Figure 10. While the foot contacts the ground, the height and velocity of contacting points (circles) are zero. In contrast, the height of other points (triangles) on the foot is greater than zero.

Therefore, the ground penetration constraints are formulated as follows:

$$\begin{aligned} &y_i(t) = 0, \quad \dot{x}_i(t) = 0, \quad \dot{y}_i(t) = 0, \quad \dot{z}_i(t) = 0, \quad i \in \Omega \\ &y_i(t) > 0, \quad i \notin \Omega, \quad 0 \leqslant t \leqslant T \end{aligned} \tag{29}$$

where Ω is the set of contacting points as illustrated in Table II.

(4) *Dynamic balance*: The dynamic balance is achieved by enforcing the ZMP to remain within the foot support polygon (FSP) as depicted in Figure 11, where $\boldsymbol{\Gamma}$ is a vector along the boundary of FSP and $\mathbf{r}$ is the position vector from a vertex of the FSP to ZMP.

DOI: 10.1002/nme

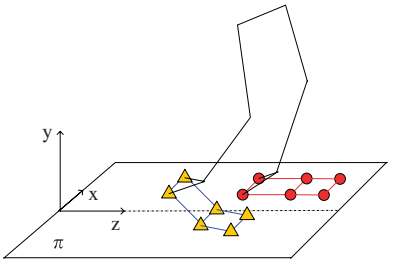

Figure 10. Foot ground penetration conditions.

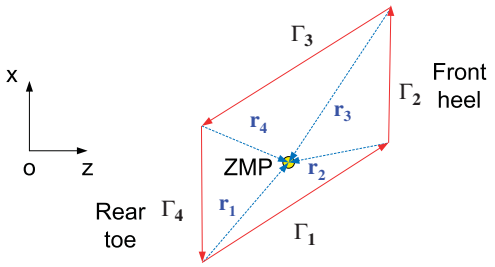

Figure 11. Foot support polygon (top view).

The ZMP constraint is mathematically expressed as follows:

$$(\mathbf{r}_i \times \mathbf{\Gamma}_i) \cdot \mathbf{n}_y \leqslant 0, \quad i = 1, \ldots, 4 \tag{30}$$

where $\mathbf{n}_y$ is the unit vector along the y axis.

(5) *Arm–leg coupling*: The arm swing is generally considered to help balance the upper body during walking to reduce the trunk moment in the vertical direction. In practice, it is difficult to measure the moment produced by the swing arm. In this study, we introduced a two-pendulum model to represent arm–leg coupling kinematics during the walking motion. The basic idea of the arm–leg coupling constraint is that the arm swing on one side counteracts the leg swing on the other side as depicted in Figure 12, where the first pendulum $\boldsymbol{\eta}_1$ represents left arm (from left shoulder to left wrist), and the second pendulum $\boldsymbol{\eta}_2$ denotes right leg (from right hip to right ankle).

The mathematical form of coupling constraint is written as

$$(\boldsymbol{\eta}_1 \cdot \mathbf{n}_z)(\boldsymbol{\eta}_2 \cdot \mathbf{n}_z) \geqslant 0 \tag{31}$$

where $\mathbf{n}_z$ is the unit vector along the z axis. It is important to note that the arm–leg coupling constraint is imposed only on the swing directions of the arm and the leg rather than a quantitative relationship on the swing angles. The swing angles are determined in the optimization process.

(6) *Self avoidance*: Self avoidance is considered in the current formulation to prevent penetration of the arm in the body. A sphere filling algorithm is used to formulate this constraint as shown in Figure 13:

$$d(\mathbf{q}, t) - r_1 - r_2 \geqslant 0, \quad 0 \leqslant t \leqslant T \tag{32}$$

DOI: 10.1002/nme

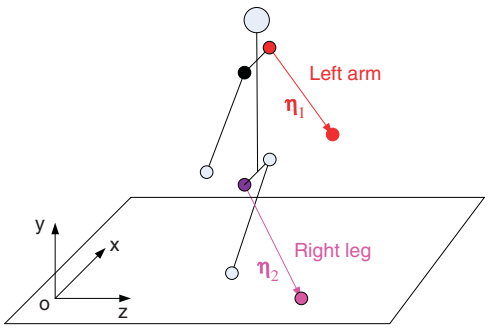

Figure 12. Arm–leg coupling motion.

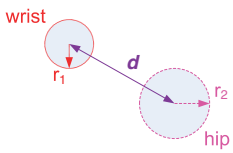

Figure 13. Self avoidance constraint between the wrist and hip.

where r_1 is a constant radius to represent the wrist, and r_2 is another radius to represent the hip; d is the distance between wrist and hip.

5.3.2. Time-independent constraints. (1) *Symmetry conditions*: The gait simulation starts from the left heel strike and ends with the right heel strike. The initial and final postures and velocities should satisfy the symmetry conditions to generate continuous walking motion. These conditions are expressed as follows:

$$\begin{aligned} q_L(0)-q_R(T)=0, \quad \dot{q}_L(0)-\dot{q}_R(T)=0 \\ q_{Sx}(0)-q_{Sx}(T)=0, \quad \dot{q}_{Sx}(0)-\dot{q}_{Sx}(T)=0 \\ q_{Sy}(0)+q_{Sy}(T)=0, \quad \dot{q}_{Sy}(0)+\dot{q}_{Sy}(T)=0 \\ q_{Sz}(0)+q_{Sz}(T)=0, \quad \dot{q}_{Sz}(0)+\dot{q}_{Sz}(T)=0 \end{aligned} \tag{33}$$

where subscripts L and R represent the DOFs of the leg, and arm and shoulder joints which satisfy the symmetry conditions with the contra-lateral leg, arm and shoulder joints; the subscript S represents the DOFs of spine, neck and global joints which satisfy the symmetry conditions on itself at the initial and final times; x, y, z are the global axes.

(2) *Ground clearance*: To avoid foot drag motion, ground clearance constraint is imposed during the walking motion. Instead of controlling the maximum height of the swing leg, the value of knee flexion at mid-swing is used to formulate ground clearance constraint. Biomechanical experiments have shown that the knee flexion of normal gait at mid-swing is around 60° regardless of the

DOI: 10.1002/nme

subjects age, and gender. This constraint is expressed as

$$-\varepsilon \leqslant q_{\text{knee}}(t) - 60 \leqslant \varepsilon, \quad t = t_{\text{mid-swing}} \tag{34}$$

where ε is a small range of motion, i.e. $\varepsilon = 5^\circ$.

(3) *Initial and final foot contacting position*: Since the step length L is given, the foot initial and final contacting positions are specified at the initial and final times to satisfy the step length constraint. It is noted that the initial and final postures and velocities are determined by the optimization process instead of specifying them from the experiments.

$$\begin{aligned} \mathbf{x}_i(0) &= \tilde{\mathbf{x}}_i(0) \\ \mathbf{x}_i(T) &= \tilde{\mathbf{x}}_i(T), \quad i \in \Omega \end{aligned} \tag{35}$$

where $\tilde{\mathbf{x}}_i$ is the specified initial and final contacting position, and Ω is the set of contacting points as specified in Table II.

6. NUMERICAL DISCRETIZATION

For the optimization problem, the time domain is discretized by using cubic B-spline curves which are defined by a set of control points $\mathbf{P}$ and time grid points (knots) $\mathbf{t}$. A joint profile $q(t)$ is parameterized by using B-splines as follows:

$$q(\mathbf{t}, \mathbf{P}) = \sum_{i=1}^{m} B_i(\mathbf{t}) p_i, \quad 0 \leqslant t \leqslant T \tag{36}$$

where $B_i(\mathbf{t})$ are the basis functions, $\mathbf{t} = \{t_0, \ldots, t_s\}$ is the knot vector, and $\mathbf{P} = \{p_1, \ldots, p_m\}$ is the control points vector. With this representation, the control points become the optimization variables (also called the design variables).

As q, $\dot{q}$, and $\ddot{q}$ are functions of $\mathbf{t}$ and $\mathbf{P}$, torque $\tau = \tau(\mathbf{t}, \mathbf{P})$ is an explicit function of the knot vector and control points. Thus, the derivatives of a torque with respect to the control points can be computed using the chain rule as

$$\frac{\partial \tau}{\partial P_i} = \frac{\partial \tau}{\partial q}\frac{\partial q}{\partial P_i} + \frac{\partial \tau}{\partial \dot{q}}\frac{\partial \dot{q}}{\partial P_i} + \frac{\partial \tau}{\partial \ddot{q}}\frac{\partial \ddot{q}}{\partial P_i} \tag{37}$$

In this study, multiplicity is used in the knot vector at the end points of the time interval. This property guarantees that the starting and ending joint angle values of a DOF are exactly those corresponding to first and the last control point values. This makes it easier to impose the symmetric posture constraints. The time-dependent constraints are imposed not only at the knot points but also between the knots, so that a very smooth motion is generated.

7. NUMERICAL RESULTS

A SQP algorithm in SNOPT [31] is used to solve the non-linear optimization problem of normal walking. To use the algorithm, cost and constraint functions and their gradients need to be calculated. The foregoing recursive kinematics and dynamics procedures provide accurate gradients

DOI: 10.1002/nme

to improve computational efficiency of the optimization algorithm. Appropriate normal walking parameters (velocity and step length) are obtained from biomechanics literature [32]. In addition to normal walking, the current work also considers situations where people walk and carry backpacks with various weights (20, 40, and 80 lbs, respectively).

7.1. Normal walking

In solving a normal gait motion, the user inputs normal walking velocity $V = 1.2\,\text{m/s}$ and step length $L = 0.6\,\text{m}$. There are 330 design variables (55 DOFs, each with six control points) and 1036 non-linear constraints. First the optimization problem is solved to obtain a feasible solution for the walking problem. Here $\mathbf{q} = \mathbf{0}$ is used as the starting point with $F(\mathbf{q}) = \text{constant}$ as the objective function and all constraints imposed. This is a new procedure for obtaining feasible solutions for a non-linear programming problem that has proved to be very effective in testing feasibility of the predictive dynamics formulation. Once a feasible solution has been obtained, it is used as the starting point for the optimization problem with dynamic effort as the objective function. There are two advantages of obtaining a feasible solution first: one is to test the feasibility of the problem formulation; and the second is to obtain a good starting point for the optimization problem. The optimality and feasibility tolerances are both set to $\varepsilon = 10^{-3}$ for SNOPT and the optimal solution is obtained in 512 CPU seconds on a Pentium(R) 4, 3.46 GHz computer. There are 158 active constraints at the optimal solution.

Figure 14 shows the resulting stick diagram of a 3D human walking on level ground including the motion in single support phase and double support phase. As expected, correct knee bending occurs to avoid collision with the ground. The arms swing to balance the leg swing. The continuity condition is satisfied to generate smooth walking motion where the initial and final postures are also optimized. ZMP location is also plotted in the figure and it stays in the FSP to satisfy the dynamic balance condition. It is important to note that the spine keeps upright automatically to reduce energy expenditure of the walking motion.

7.2. Validation of normal walking

7.2.1. Kinematics. Based on the human gait literature, six kinematics variables (angles and displacements) have been chosen as determinants to define forward walking [33]. These determinants correspond to the lower extremities and pelvic motion: hip flexion/extension, knee flexion/extension, ankle plantar/dorsiflexion, pelvic tilt, pelvic rotation, and lateral pelvic displacement.

The walking motion experimental data, collected by the authors, are comprised of four healthy male subjects. During the walking trials, each subject walked at a self-selected speed. The experimental data for each subject were also normalized by dividing the cycle time to directly evaluate the determinants at a percentage of a gait cycle. For each subject, the time scale was normalized such that the initial left heel strike occurred at time $t = 0$ and the subsequent left heel strike occurred at time $t = 1$ [34].

The predicted six determinants of normal walking for a stride starting from heel strike and ending with the same heel strike are plotted in Figure 15. The solid curves in the figure represent the predicted determinants, the dashed curves are experimental mean value of the determinants, and the dotted curves show 95% confidence region of the statistical means. In general, the predicted walking motion has shown a strong correlation with the experimental data. The six simulated determinants lie close to the mean of the experimental data; major parts of the

DOI: 10.1002/nme

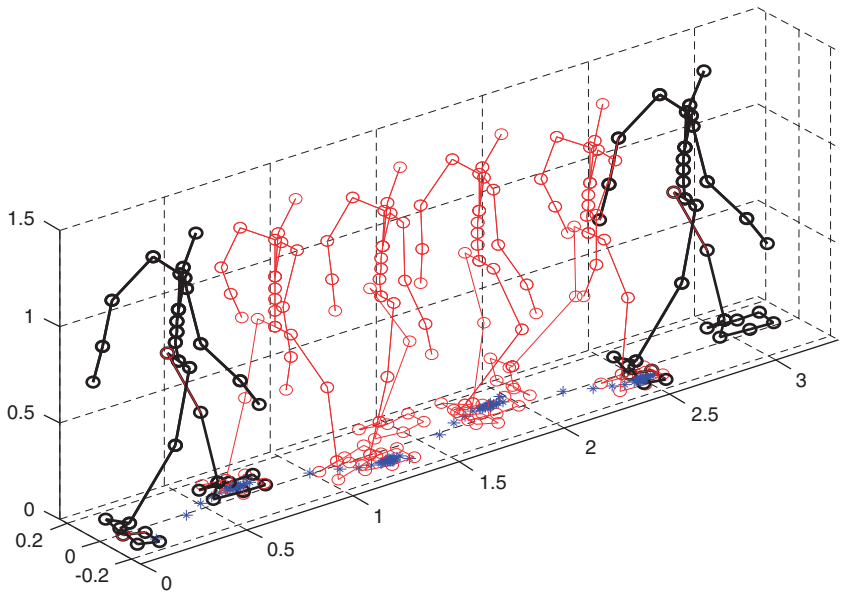

Figure 14. The diagram of optimized cyclic walking motion (two strides).

motion are in the confidence region and have similar trends as the statistical mean. The peak values of ankle motion, pelvic rotation, and pelvic lateral displacement occur earlier than the experimental data. This is because the six determinants represent a complex coupled motion, and the optimal solution is only a compromise motion. Furthermore, ankle motion is the major passive movement due to GRF. It has shown a larger plantar flexion at 60% of gait cycle. These differences are expected due to approximations in the mechanical model of the human body.

7.2.2. Dynamics. Since we are using a rigid skeleton model, the energy absorption of muscle tendon-ligament and joint tissue are ignored at heel strike and toe-off. This results in some jerks in GRF and joint torques. Therefore, the Butterworth low-pass filter with cutting frequency of 8 Hz is used to obtain plots for the GRF and joint torques. Figure 16 depicts torque profiles of the hip, the knee and the ankle for a stride. Here, HS denotes heel strike, FF foot flat, HO heel off, and TO toe-off. The figure also shows torques data (digitized) obtained from the literature [35, 36].

In Figure 16, the hip torque begins to flex the hip at the heel strike and this torque reaches its maximum extension torque at terminal stance phase. At the knee joint, the reaction force flexes the knee during early stance, but the knee torque then reverses into an extension torque. Before the swing phase, the knee is flexed for a second time. The ankle starts with a plantar torque just after heel strike and reverses into a dorsiflexion torque continuously during stance, reaching peak at terminal stance and then dropping quickly until toe-off.

Figure 17 shows the GRF for the predicted walking motion. The vertical GRF has a familiar double-peak pattern, and the maximum vertical force is developed soon after heel strike and then again during terminal stance (push off). In the walking direction, the fore–aft GRF, there is a

DOI: 10.1002/nme

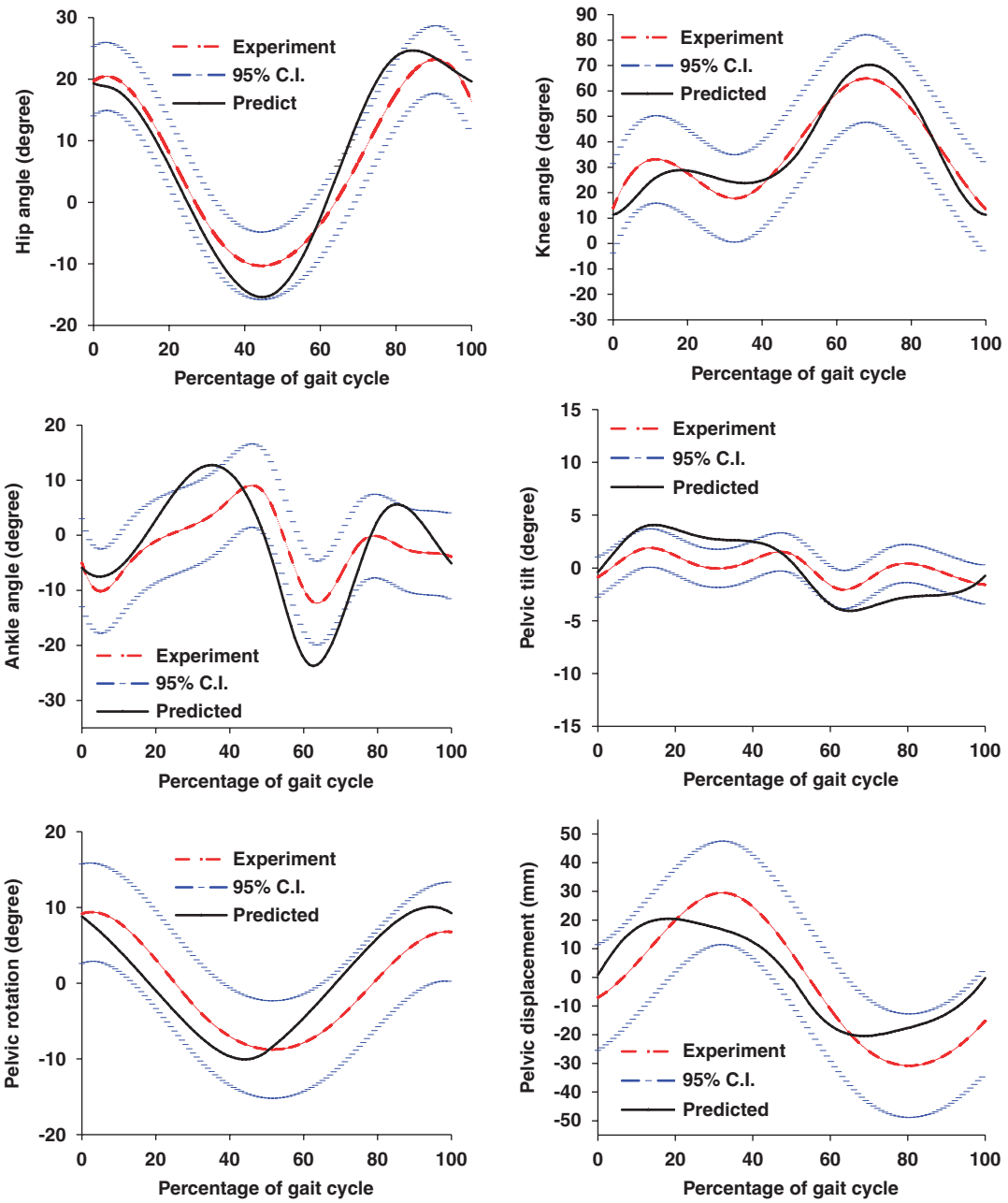

Figure 15. Comparison of predicted determinants with the experimental data.

DOI: 10.1002/nme

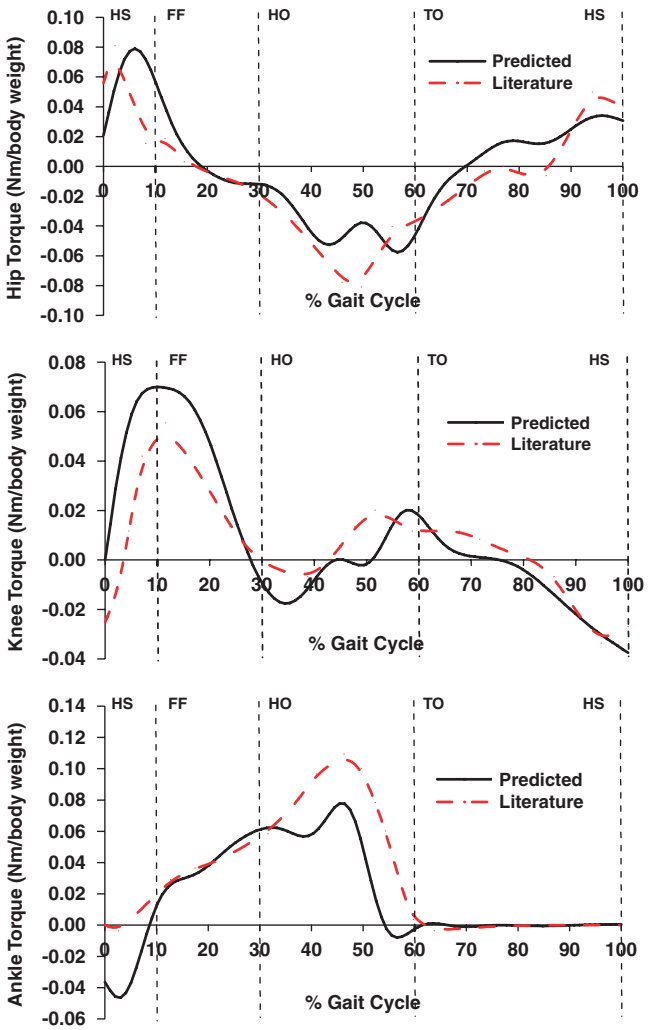

Figure 16. Joint torque profiles for a stride.

decelerating force early in the stance phase, and an acceleration force at push off. Meanwhile, the foot also pushes laterally during the entire stance phase.

The above resulting joint torques and GRF have shown general agreement with the experimental results presented in the literature [35, 36]. However, there are discrepancies at the beginning and end of the gait cycle. Since we do not impose symmetry conditions on joint angle accelerations, the predicted forces show impact phenomena with discontinuities at the boundaries. The discrepancies may also be due to approximate simulation of impacts during walking motion. In addition, the GRF are linearly distributed between the feet during the double support phase and this may also result in some inaccuracies.

DOI: 10.1002/nme

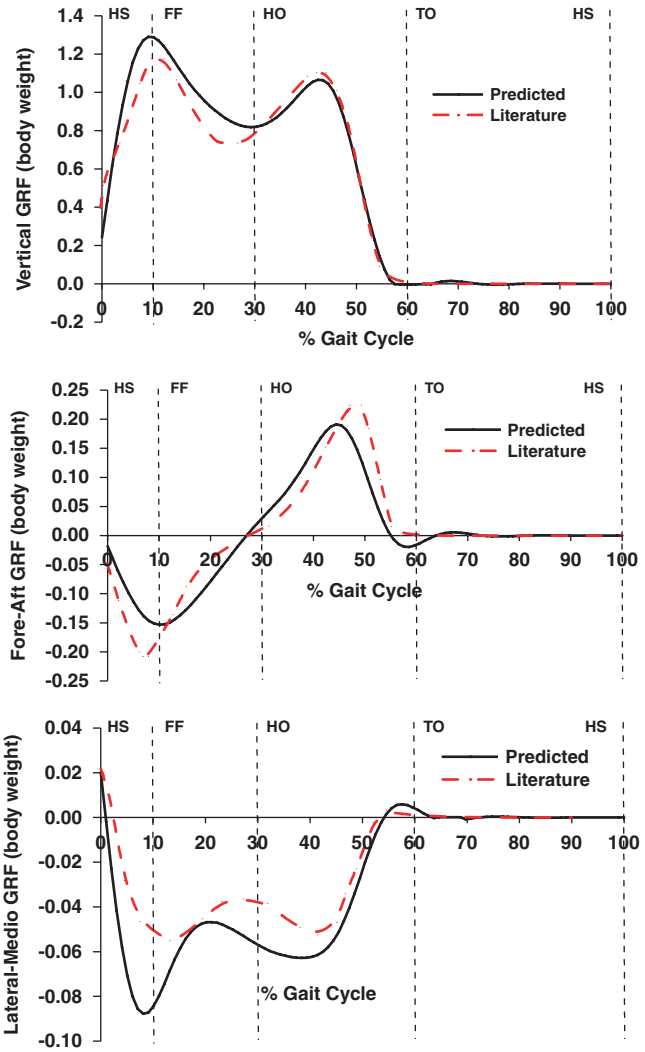

Figure 17. Ground reaction forces for a stride.

7.3. *Walking with backpack*: *cause-and-effect*

Next a backpack is considered for simulation of the walking motion with the walking velocity $V = 1.2\,\mathrm{m/s}$ and step length $L = 0.6\,\mathrm{m}$. The backpack is considered as a point load applied on the back in the downward vertical direction. Although this backpack model is relatively simple, it is used to study its cause-and-effect during the gait cycle. Three cases are simulated with varying backpack weights: 20, 40, and 80 lbs. 3D stick diagrams of the walking motion are compared in Figure 18 and a reasonable spine bending is observed with increasing backpack weight. The joint angle profiles, the GRF, and the joint torque profiles are illustrated in Figures 19, 20, and 21, respectively.

DOI: 10.1002/nme

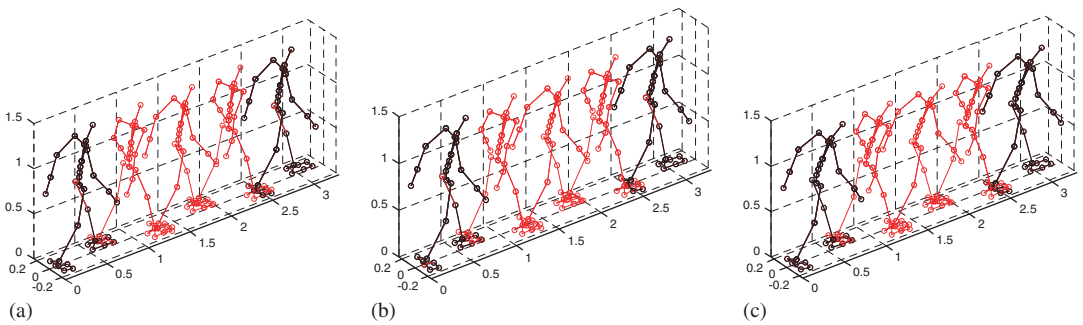

Figure 18. Optimized walking motion with backpack: (a) 20 lb; (b) 40 lb; and (c) 80 lb.

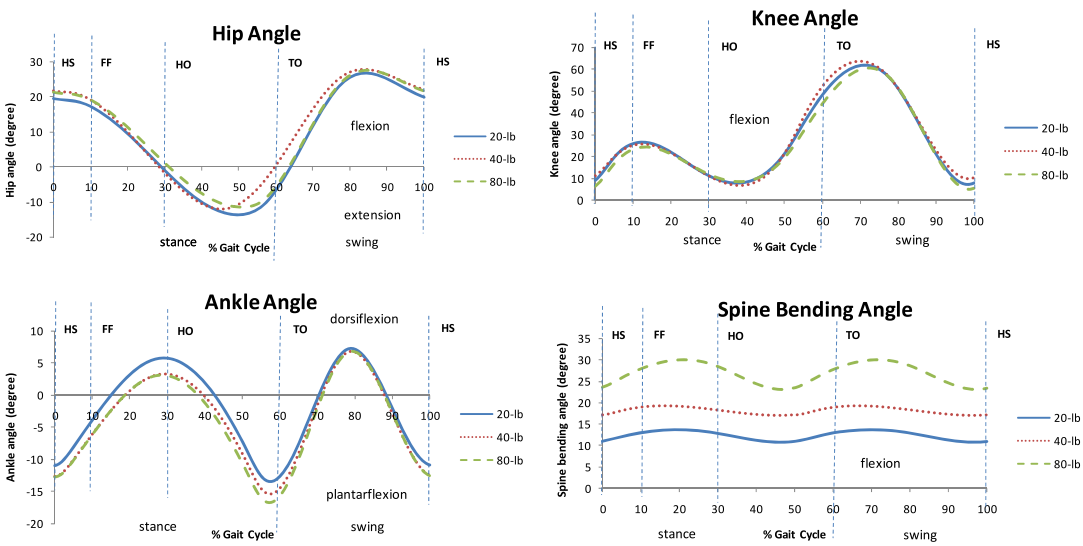

Figure 19. Joint profiles with backpack.

The hip, knee, and ankle motions have no significant differences with different backpacks. This is because they are all simulated with the same walking velocity and step length. However, the spine bending angles are significantly affected by the backpack weights. Heavier weight results in larger spine bent to lower the center of mass and increase stability.

The GRF show generally larger forces with increasing backpack weight. There is a significant backpack effect on the vertical GRF. For the fore–aft GRF, the 80-lb backpack results in greater minimum and maximum force than the 20-lb backpack. The 40-lb backpack has a minimum force similar to the 20-lb backpack and a maximum force similar to the 80-lb backpack. For medial–lateral GRF, the 80-lb backpack has larger peak force compared with 20-lb and 40-lb backpacks; however, there is no significant difference in other parts of the gait cycle.

It is seen that the torques on the lower extremity are almost the same in the swing phase, however, they are different in the stance phase because of varying weight of the backpack. In the

DOI: 10.1002/nme

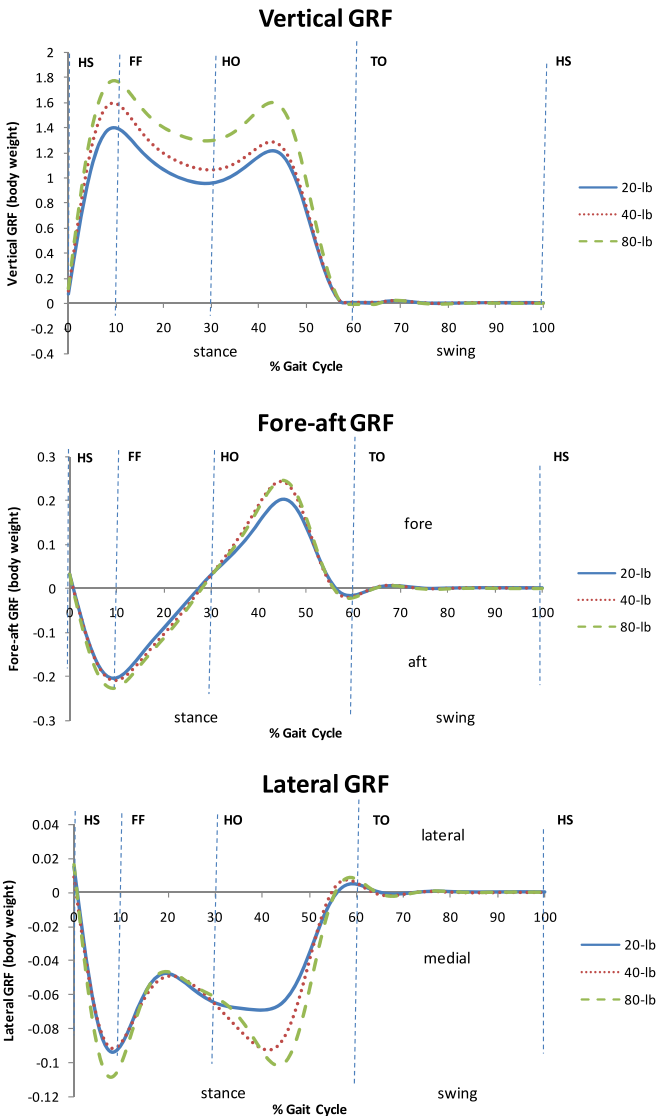

Figure 20. Ground reaction forces with backpack.

swing phase, all the weight is shifted to the supporting leg, hence, the torque of the swinging leg is almost the same with different backpacks. This is quite reasonable. On the other hand, during the stance phase, 80-lb backpack results in larger peak torque compared with 20-lb and 40-lb backpacks. For the hip and knee torques, there is no significant difference between 20-lb and 40-lb backpacks. The maximum extension knee torque of 80-lb backpack is similar to those of other backpacks, but the maximum flexion torque occurs later than that for the lighter backpacks. The spine bending torque shows significant larger value with increase of the backpack weight.

DOI: 10.1002/nme

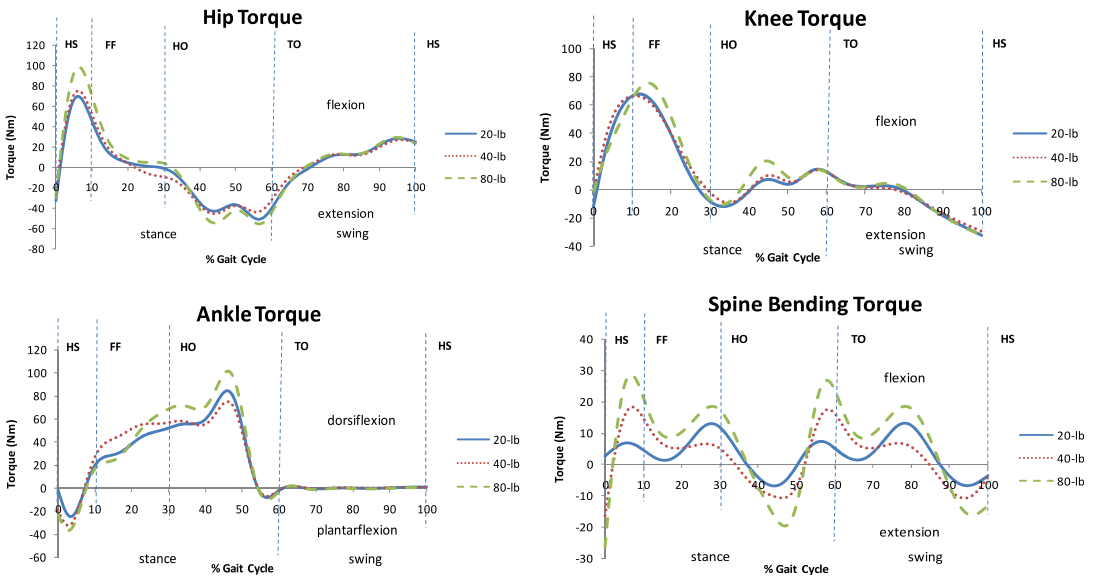

Figure 21. Joint torque profiles with backpack.

An interesting result is observed from the foregoing analyses. Different weight backpacks are considered with the same walking parameters (step length and velocity). Therefore, similar joint profiles of the lower extremities are obtained with different backpacks. Although, the GRF have significant differences, especially for the vertical GRF, the joint torque profiles have no significant differences. This may be explained in the context of human walking strategy; the GRF location is optimized to facilitate an energy saving walk for different backpacks to increase stability and reduce the joint torques. Thus, the current algorithm predicts that people will choose a strategy to walk more efficiently for carrying backpacks under the given walking parameters.

8. CONCLUDING REMARKS

In this paper, a formulation to predict normal walking motion of a 55-DOF digital human model was presented. The normal walking was treated as a cyclic and symmetric motion with repeatable initial and final postures and velocities. The motion planning was formulated as a large-scale non-linear programming problem that was solved using the sequential quadratic programming algorithm. Joint profiles were discretized using cubic B-splines and the corresponding control points were treated as unknowns. The energy-related objective function, integral of squares of all joint torques, was minimized. Owing to its crucial role in walking, the arm motion was incorporated by considering the arm–leg motion coupling constraint in the formulation. A novel two-step algorithm was presented to calculate ground reaction forces (GRF) and the ZMP using the equations of motion. A new approach to obtain just the feasible solutions for the walking problem was presented and used effectively. Data for the six standard walking determinants were obtained from experiments with human subjects and were used to verify the simulated gait motion. The effect

DOI: 10.1002/nme

of external force, such as backpacks, on gait motion was studied and reasonable simulations were obtained. The current formulation was shown to be very effective in obtaining joint torques and GRF. Furthermore, the current methodology was found to be quite robust due to the significant role of the analytical gradients which were calculated using recursive Lagrangian dynamics. Finally, the proposed skeletal model, problem formulation and the solution procedure predicted both kinematics and dynamics of human walking quite accurately. Furthermore, the formulation is flexible where the effect of external loads on the body segments and various constraints can be studied in a systematic way.

APPENDIX A

Major joint angle limits are given in Table AI.

Table AI. Major joint angle limits.*,†

	Joint angle limits (degree)	
Joints	Lower limit	Upper limit
Ankle (dorsi/plantar)	−20	55
Knee (extension/flexion)	0	138
Hip (flexion/extension)	−102	41
Hip (abduct/adduct)	−46	34
Hip (external/internal)	−49	32
Lumbar spine (tilt)	−25	25
Lumbar spine (extension/flexion)	−30	75
Lumbar spine (rotation)	−30	30
Shoulder (extension/flexion)	−60	180
Shoulder (abduct/adduct)	−180	45
Elbow (flexion/extension)	−140	0

*Zero joint angles correspond to home configuration as depicted in Figure 2.
†Joint coupling motion are not considered.

ACKNOWLEDGEMENTS

This research was supported by project from TACOM and the Soldier Systems Center (Natick).

REFERENCES

1. Choi MG, Lee J, Shin SY. Planning biped locomotion using motion capture data and probabilistic roadmaps. *Acm Transactions on Graphics* 2003; **22**(2):182–203.
2. Pettre J, Laumond JP. A motion capture-based control-space approach for walking mannequins. *Computer Animation and Virtual Worlds* 2006; **17**(2):109–126.

DOI: 10.1002/nme

3. Yamaguchi J, Soga E, Inoue S, Takanishi A. Development of a bipedal humanoid robot control method of whole body cooperative dynamic biped walking. *IEEE International Conference on Robotics and Automation*, Detroit, MI, U.S.A., 1999; 368–374.
4. Kajita S, Kanehiro F, Kaneko K, Fujiwara K, Harada K, Yokoi K, Hirukawa H. Biped walking pattern generation by using preview control of zero-moment point. *IEEE International Conference on Robotics and Automation*, Taipei, Taiwan, 2003; 1620–1626.
5. Huang Q, Yokoi K, Kajita S, Kaneko K, Arai H, Koyachi N, Tanie K. Planning walking patterns for a biped robot. *IEEE Transactions on Robotics and Automation* 2001; **17**(3):280–289.
6. Mu X, Wu Q. Synthesis of a complete sagittal gait cycle for a five-link biped robot. *Robotica* 2003; **21**:581–587.
7. Kim HJ, Horn E, Arora JS, Abdel-Malek K. An optimization-based methodology to predict digital human gait motion. *Digital Human Modeling for Deisgn and Engineering Symposium*, Iowa City, IA, U.S.A., 2005.
8. Park JH, Kim KD. Biped robot walking using gravity-compensated inverted pendulum mode and computed torque control. *IEEE International Conference on Robotics and Automation*, Leuven, Belgium, 1998; 3528–3533.
9. Chevallereau C, Aoustin Y. Optimal reference trajectories for walking and running of a biped robot. *Robotica* 2001; **19**:557–569.
10. Saidouni T, Bessonnet G. Generating globally optimised sagittal gait cycles of a biped robot. *Robotica* 2003; **21**:199–210.
11. Anderson FC, Pandy MG. Dynamic optimization of human walking. *Journal of Biomechanical Engineering—Transaction of the ASME* 2001; **123**(5):381–390.
12. Lo J, Huang G, Metaxas D. Human motion planning based on recursive dynamics and optimal control techniques. *Multibody System Dynamics* 2002; **8**(4):433–458.
13. Fregly BJ, Reinbolt JA, Rooney KL, Mitchell KH, Chmielewski TL. Design of patient-specific gait modifications for knee osteoarthritis rehabilitation. *IEEE Transactions on Bio-Medical Engineering* 2007; **54**(9):1687–1695.
14. Ren L, Jones RK, Howard D. Predictive modelling of human walking over a complete gait cycle. *Journal of Biomechanics* 2007; **40**(7):1567–1574.
15. Kim HJ, Wang Q, Rahmatalla S, Swan CC, Arora JS, Abdel-Malek K, Assouline JG. Dynamic motion planning of 3D human locomotion using gradient-based optimization. *Journal of Biomechanical Engineering* 2008; **130**(3):031002.
16. Xiang Y, Chung JH, Kim JH, Bhatt R, Marler RT, Rahmatalla S, Yang J, Arora JS, Abdel-Malek K. Predictive dynamics: an optimization-based novel approach for human motion simulation. *Structural and Multidisciplinary Optimization* 2009 (in review).
17. Denavit J, Hartenberg RS. A kinematic notation for lower-pair mechanisms based on matrices. *ASME Journal of Applied Mechanics* 1955; **22**:215–221.
18. Cheng H, Obergefell L, Rizer A. Generator of body (GEBOD) manual. *AL/CF-TR-1994–0051*, Armstrong Laboratory, Wright-Patterson Air Force Base, Ohio, 1994.
19. Uicker JJ. *On the Dynamic Analysis of Spatial Linkages using 4×4 Matrices*. Northwestern University: Evanston, 1965.
20. Hollerbach JM. A recursive Lagrangian formulation of manipulator dynamics and a comparative-study of dynamics formulation complexity. *IEEE Transactions on Systems, Man, and Cybernetics* 1980; **10**(11):730–736.
21. Toogood RW. Efficient robot inverse and direct dynamics algorithms using micro-computer based symbolic generation. *IEEE International Conference on Robotics and Automation*, Scottsdale, AZ, U.S.A., 1989; 1827–1832.
22. Xiang Y, Arora JS, Abdel-Malek K. Optimization-based motion prediction of mechanical systems: sensitivity analysis. *Structural and Multidisciplinary Optimization* 2009; **37**(6):595–608.
23. Vukobratović M, Borovac B. Zero-moment point—thirty five years of its life. *International Journal of Humanoid Robotics* 2004; **1**(1):157–173.
24. Goswami A. Postural stability of biped robots and the foot-rotation indicator (FRI) point. *International Journal for Robotics Research* 1999; **18**(6):523–533.
25. Sardain P, Bessonnet G. Forces acting on a biped robot. Center of pressure-zero moment point. *IEEE Transactions on Systems, Man, and Cybernetics A* 2004; **34**(5):630–637.
26. Dasgupta A, Nakamura Y. Making feasible walking motion of humanoid robots from human motion capture data. *IEEE International Conference on Robotics and Automation*, Detroit, MI, U.S.A., 1999; 1044–1049.
27. Ayyappa E. Normal human locomotion, part 1: basic concepts and terminology. *Journal of Prosthetics and Orthotics* 1997; **9**(1):10–17.
28. Cahalan TD, Johnson ME, Liu S, Chao EYS. Quantitative measurements of hip strength in different age-groups. *Clinical Orthopaedics and Related Research* 1989; **R**(246):136–145.

DOI: 10.1002/nme

29. Kaminski TW, Perrin DH, Gansneder BM. Eversion strength analysis of uninjured and functionally unstable ankles. *Journal of Athletic Training* 1999; **34**(3):239–245.
30. Kumar S. Isolated planar trunk strengths measurement in normals.3. Results and database. *International Journal of Industrial Ergonomics* 1996; **17**(2):103–111.
31. Gill PE, Murray W, Saunders MA. SNOPT: an SQP algorithm for large-scale constrained optimization. *SIAM Journal on Optimization* 2002; **12**(4):979–1006.
32. Inman VT, Ralston RJ, Todd F. *Human Walking*. Wilkins & Wilkins: Baltimore, MD, 1981.
33. Saunders JBDM, Inman VT, Eberhart HD. The major determinants in normal and pathological gait. *Journal of Bone and Joint Surgery* (*American*) 1953; **35-A**(3):543–558.
34. Rahmatalla S, Xiang Y, Smith R, Li J, Muesch J, Bhatt R, Swan CC, Arora JS, Abdel-Malek K. A validation protocol for predictive human locomotion. *2008 Digital Human Modeling for Design and Engineering Symposium*, Pittsburgh, PA, U.S.A., 2008.
35. Stansfield BW, Hillman SJ, Hazlewood ME, Robb JE. Regression analysis of gait parameters with speed in normal children walking at self-selected speeds. *Gait Posture* 2006; **23**(3):288–294.
36. Simpson KJ, Jiang P. Foot landing position during gait influences ground reaction forces. *Clinical Biomechanics* 1999; **14**(6):396–402.

DOI: 10.1002/nme